Dynamic response of modulators based on cascaded-ring-resonator

Suguru Akiyama[1,2,*] and Shintaro Nomura[2]

[1]*Fujitsu Laboratories Ltd. 10-1 Morinosato-Wakamiya, 243-0122, Japan*
[2]*Graduate School of Pure and Applied Sciences, University of Tsukuba, 1-1-1 Tennoudai, Tsukuba 305-8571, Japan*
[*]*akiyama.suguru@jp.fujitsu.com*

Abstract: We investigated the dynamic response of a cascaded-ring-resonator-loaded Mach–Zehnder modulator (CRR-MZM), in which a number of cascaded ring resonators (RRs) are loaded in the interferometer as phase modulators. The analytical form is derived for the small-signal response of CRR-MZM using temporal-coupled-mode (TCM) theory, and its validity is confirmed by numerical calculations. It is revealed that the bandwidth of the CRR-MZM is maximized by setting proper delays in driving signals between neighboring RRs; the optimized delay is twice the photon lifetime of each RR. The calculated performances of CRR-MZMs are compared with those of standard modulators based on a single-ring-resonator (SRR) without interferometer, in terms of the modulation depth and bandwidth. For a given degree of the refractive index change in a waveguide, CRR-MZM can provide a larger modulation depth than a SRR-type modulator in frequency ranges exceeding 25 GHz.

OCIS codes: (250.4110) Modulators; (250.7360) Waveguide modulators; (230.5750) Resonators; (250.5300) Photonic integrated circuits.

References and links

1. D. A. B. Miller, "Device requirements for optical interconnects to silicon chips," Proc. IEEE **97**(7), 1166–1185 (2009).
2. Q. Xu, S. Manipatruni, B. Schmidt, J. Shakya, and M. Lipson, "12.5 Gbit/s carrier-injection-based silicon micro-ring silicon modulators," Opt. Express **15**(2), 430–436 (2007).
3. P. Dong, S. Liao, H. Liang, W. Qian, X. Wang, R. Shafiiha, D. Feng, G. Li, X. Zheng, A. V. Krishnamoorthy, and M. Asghari, "High-speed and compact silicon modulator based on a racetrack resonator with a 1 V drive voltage," Opt. Lett. **35**(19), 3246–3248 (2010).
4. J. Rosenberg, W. M. Green, A. Rylyakov, C. Schow, S. Assefa, B. G. Lee, C. Jahnes, and Y. Vlasov, "Ultra-low-voltage micro-ring modulator integrated with a CMOS feed-forward equalization driver," in *Optical Fiber Communication Conference, OSA Technical Digest* (CD) (Optical Society of America, 2011), paper OWQ4 (2011).
5. W. D. Sacher, W. M. J. Green, S. Assefa, T. Barwicz, S. M. Shank, Y. A. Vlasov, and J. K. S. Poon, "Controlled coupling in silicon microrings for high-speed, high extinction ratio, and low-chirp modulation," in *Conference on Lasers and Electro-Optics / Quantum Electronics and Laser Science Conference* (CLEO/QELS 2011), paper PDPA8 (2011).
6. J. C. Rosenberg, W. M. J. Green, S. Assefa, T. Barwicz, M. Yang, S. M. Shank, and Y. A. Vlasov, "Low-power 30 Gbps silicon microring modulator," in *Conference on Lasers and Electro-Optics / Quantum Electronics and Laser Science Conference* (CLEO/QELS 2011), paper PDPB9 (2011).
7. G. Li, X. Zheng, J. Yao, H. Thacker, I. Shubin, Y. Luo, K. Raj, J. E. Cunningham, and A. V. Krishnamoorthy, "25Gb/s 1V-driving CMOS ring modulator with integrated thermal tuning," Opt. Express **19**(21), 20435–20443 (2011).
8. S. Akiyama, T. Kurahashi, T. Baba, N. Hatori, T. Usuki, and T. Yamamoto, "A 1V peak-to-peak driven 10-Gbps slow-light silicon Mach-Zehnder modulator using cascaded ring resonators," Appl. Phys. Express **3**(7), 072202 (2010).
9. D. M. Gill, S. S. Patel, M. Rasras, K. Y. Tu, A. E. White, Y. K. Chen, A. Pomerene, D. Carothers, R. L. Kamocsai, C. M. Hill, and J. Beattie, "CMOS-compatible Si-ring-assisted Mach-Zehnder interferometer with internal bandwidth equalization," IEEE J. Sel. Top. Quantum Electron. **16**(1), 45–52 (2010).
10. S. Akiyama, T. Kurahashi, K. Morito, T. Yamamoto, T. Usuki, and S. Nomura, "Cascaded-ring-resonator-loaded Mach-Zehnder modulator for enhanced modulation efficiency in wide optical bandwidth," Opt. Express **20**(15), 16321–16338 (2012).

#172056 - $15.00 USD Received 5 Jul 2012; revised 23 Aug 2012; accepted 23 Aug 2012; published 10 Sep 2012

11. A. M. Gutierrez, A. Brimont, G. Rasigade, M. Ziebell, D. Marris-Morini, J.-M. Fedeli, L. Vivien, J. Marti, and P. Sanchis, "Ring-assisted Mach–Zehnder interferometer silicon modulator for enhanced performance," J. Lightwave Technol. **30**(1), 9–14 (2012).
12. H. C. Nguyen, Y. Sakai, M. Shinkawa, N. Ishikura, and T. Baba, "10 Gb/s operation of photonic crystal silicon optical modulators," Opt. Express **19**(14), 13000–13007 (2011).
13. A. Brimont, D. J. Thomson, P. Sanchis, J. Herrera, F. Y. Gardes, J. M. Fedeli, G. T. Reed, and J. Martí, "High speed silicon electro-optical modulators enhanced via slow light propagation," Opt. Express **19**(21), 20876–20885 (2011).
14. H. Tazawa, Y. Kuo, I. Dunayevskiy, J. Luo, A. K. Y. Jen, H. Fetterman, and W. Steier, "Ring resonator based electrooptic polymer traveling-wave modulator," J. Lightwave Technol. **24**(9), 3514–3519 (2006).
15. H. Kaneshige, Y. Ueyama, H. Yamada, T. Arakawa, and Y. Kokubun, "Quantum well Mach-Zehnder modulator with single microring resonator and optimized arm length," 17th Microoptics Conference (MOC' 11), Sendai, Japan, paper G-5, (2011).
16. H. F. Taylor, "Enhanced electrooptic modulation efficiency utilizing slow-wave optical propagation," J. Lightwave Technol. **17**(10), 1875–1883 (1999).
17. M. Soljačić, S. G. Johnson, S. Fan, M. Ibanescu, E. Ippen, and J. D. Joannopoulos, "Photonic-crystal slow-light enhancement of nonlinear phase sensitivity," J. Opt. Soc. Am. B **19**(9), 2052–2059 (2002).
18. R. A. Soref and B. R. Bennett, "Electrooptical effects in silicon," IEEE J. Quantum Electron. **23**(1), 123–129 (1987).
19. B. E. Little, S. T. Chu, H. A. Haus, J. Foresi, and J.-P. Laine, "Microring resonator channel dropping filters," J. Lightwave Technol. **15**(6), 998–1005 (1997).
20. L. C. Kimerling, D. Ahn, A. B. Apsel, M. Beals, D. Carothers, Y.-K. Chen, T. Conway, D. M. Gill, M. Grove, C.-Y. Hong, M. Lipson, J. Liu, J. Michel, D. Pan, S. S. Patel, A. T. Pomerene, M. Rasras, D. K. Sparacin, K.-Y. Tu, A. E. White, and C. W. Wong, "Electronic-photonic integrated circuits on the CMOS platform," Proc. SPIE **6125**, 612502, 612502-10 (2006).
21. F. Xia, L. Sekaric, and Y. A. Vlasov, "Ultra-compact optical buffers on a silicon chip," Nat. Photonics **1**(1), 65–71 (2007).
22. I. L. Gheorma and R. M. Osgood, "Fundamental limitations of optical resonator based on high-speed EO modulators," IEEE Photon. Technol. Lett. **14**(6), 795–797 (2002).
23. W. D. Sacher and J. K. S. Poon, "Dynamics of microring resonator modulators," Opt. Express **16**(20), 15741–15753 (2008).
24. L. Zhang, Y. Li, J.-Y. Yang, M. Song, R. G. Beausoleil, and A. E. Willner, "Silicon-based microring resonator modulators for intensity modulation," IEEE J. Sel. Top. Quantum Electron. **16**(1), 149–158 (2010).
25. T. Ye and X. Cai, "On power consumption of silicon-microring-based optical modulators," J. Lightwave Technol. **28**(11), 1615–1623 (2010).
26. J. D. Joannopoulos, S. G. Johnson, J. N. Winn, and R. D. Meade, *Photonic Crystals: Molding the Flow of Light, second edition*, (Princeton University Press, 2008).
27. A. Yariv, "Universal relations for coupling of optical power between microresonators and dielectric waveguides," Electron. Lett. **36**(4), 321–322 (2000).
28. K. Okamoto, *Fundamentals of Optical Waveguides*, (Academic Press, 2006), Chap. 5.
29. O. Schwelb, "Transmission, group delay, and dispersion in single-ring optical resonators and add/drop filters - a tutorial overview," J. Lightwave Technol. **22**(5), 1380–1394 (2004).

1. Introduction

Optical modulators play a key role in optical communication systems by converting high-speed electrical signals into optical signals. The fundamental requirement for modulators is that they transmit a large amount of data per unit time [1]. Therefore, modulators should have wide bandwidths and operate at speeds that are as high as possible. In most applications, another important metric for modulators is power consumption [1]. It is necessary to reduce the power consumption of modulators while keeping a sufficient modulation depth. Thus, it is necessary for modulators to increase the optical response to an applied electrical signal.

The use of optical resonators has shown promise in increasing the response of modulators [2–17]. Light dwells in resonators, increasing the interaction of light with matter, and causes the enhancement of any kind of electro-optical effect [16, 17]. This approach has been actively investigated, particularly for modulators that are based on silicon [2–13]. One reason is that silicon lacks the strong electro-optical effect unlike III-V systems [18], and the use of resonators is therefore desired to enhance the modulation. The other reason is that the silicon waveguide is suitable for configuring the micrometer-scale resonators needed for modulators, due to the tight confinement of light in the waveguide [2–13, 19–21].

In particular, modulators that are based on a single micro ring resonator (RR) in an all-pass filter configuration have been extensively investigated [2–7]. They have achieved the lowest driving voltage and highest modulation speed among silicon modulators that use

#172056 - $15.00 USD Received 5 Jul 2012; revised 23 Aug 2012; accepted 23 Aug 2012; published 10 Sep 2012

resonators [6, 7]. These modulators have sharp dips in the intensity transmission spectrum at the resonant wavelengths. A tiny change in the refractive index due to the electrical input signals causes sufficient intensity variations by shifting the resonant wavelengths; we call this type of modulator a single-ring-resonator-based spectral shifting modulator (SRR-SSM). However, one drawback is becoming increasingly noticeable in the SRR-SSM as the operating speed of silicon modulators increases; they are approaching the inherent limit in operating speed associated with the photon lifetime in the RR [6, 22–25]. For a given change in refractive index, it is necessary to increase the Q value of the RR to obtain adequate modulation. This inevitably causes a large photon lifetime in the RR, and therefore limits its modulation response at high frequencies.

CRR-MZMs can be used to mitigate this problem, in which a number of RRs are cascaded and loaded in the interferometer as phase modulators [8, 10]. For a given change in the refractive index in the waveguide, it is possible to obtain a large response by increasing the Q value of the RRs and also by increasing the number of cascaded RRs. Therefore, it is expected that CRR-MZMs provide sufficient intensity modulation while maintaining wide modulation bandwidths by using CRRs with relatively low Q, and thus short lifetime. For CRR-MZMs, while performances have been reported emphasizing the modulation enhancement and optical bandwidth [10], the characteristics and limitations for high-speed operations have not yet been theoretically or experimentally investigated.

In this paper, we investigated the characteristics and limitations of a CRR-MZM in high-speed operation using analytical and numerical calculations. We first derived the analytical formula of the small-signal response of CRR-MZMs by using the temporal-coupled-mode (TCM) theory [19, 26], and confirmed its validity by way of numerical calculations. Using the analytical model, we revealed that the bandwidth of the CRR-MZM is maximized by setting proper delays in the driving signals between neighboring RRs. We compared the calculated performances of the CRR-MZM with those of a standard SRR-SSM, in terms of modulation depth and bandwidth. For a given index change in waveguides, CRR-MZM can provide modulation responses that are larger than those of SRR-SSM, with a propagation loss of 10 dB/cm, and in frequency bands that are larger than 25 GHz.

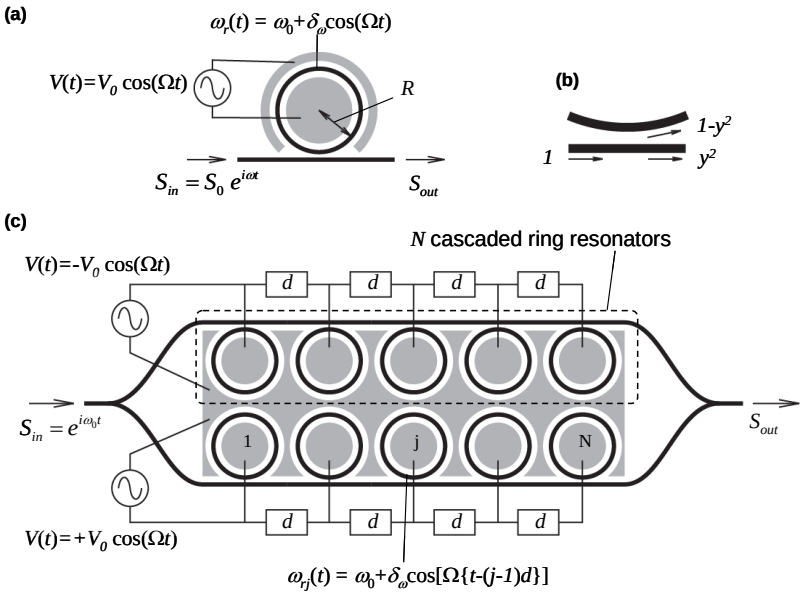

Fig. 1. Schematic view of RR-based modulators in two different configurations, and definition of parameters used in this paper. (a) SRR-SSM. (b) Coupling between ring and bus waveguide as a part of RRs. y^2 and $1 - y^2$ indicate the fraction of the power transmitted to the bus and the ring waveguide, respectively. (c) CRR-MZM. *d* indicates the time delay set in the electrical signals between two neighboring RRs.

#172056 - $15.00 USD Received 5 Jul 2012; revised 23 Aug 2012; accepted 23 Aug 2012; published 10 Sep 2012

2. Analytical modeling

In this section, we derive the analytical formula of the response of CRR-MZM for small-signal modulation. First, we start with a standard single RR without interferometer, SRR-SSM, as shown in Fig. 1(a). We used TCM theory to describe the system [19, 24–26].

$$\frac{dA(t)}{dt} = \left(i\,\omega_r(t) - \frac{1}{\tau_c} - \frac{1}{\tau_l} \right) A(t) + \sqrt{\frac{2}{\tau_c}} S_{in}(t). \tag{1}$$

$$S_{out}(t) = -S_{in}(t) + \sqrt{\frac{2}{\tau_c}} A(t). \tag{2}$$

In the above equations, $A(t)$ express the field inside the RR. $A(t)$ is oscillating at an angular frequency ω_r with a total stored energy of $|A(t)|^2$. $S_{in}(t)$ and $S_{out}(t)$ are lights that are coupled into and out of the RR, respectively. They have power flows of $|S_{in}(t)|^2$ and $|S_{out}(t)|^2$, respectively, inside the waveguide. τ_c and τ_l are the lifetimes of photons that escape from the RR by the processes of coupling out to the bus waveguide and dissipation due to waveguide loss, respectively. They are related to the usual structural parameters of RRs.

$$\frac{1}{\tau_c} = \frac{(1-y^2) v_g}{2(2\pi R)}, \quad \text{and} \tag{3a}$$

$$\frac{1}{\tau_l} = \frac{\alpha_{dB}\, v_g}{20 \log_{10} e}. \tag{3b}$$

y is defined so that $1\text{-}y^2$ indicates the fraction of power that is transferred from the bus waveguide and ring waveguide in the coupling region, as shown in Fig. 1(b). R, v_g, and α_{dB} are the radius, group velocity and attenuation constant of the ring waveguide, respectively.

Throughout this paper, we consider only the refractive index modulation of the RR, in which only the refractive index is modulated according to the electrical signal that is uniformly applied to each RR. The attenuation constant and the coupling coefficient are always constant. One may assume that the group index of the waveguide is also modulated with the refractive index, and that this may affect the behavior of the RRs through Eq. (3). However, we neglected the change of the group index, as was done in other analyses [23–25]. This is reasonable because in RR-based modulators, the modulation occurs due to the interference in the coupling region, which is governed not by the group index but by the refractive index. Thus, in our analysis, ω_r is a time-dependent function $\omega_r(t)$. When a voltage is applied to the ring resonator, the resonant frequency ω_r is modulated at a frequency of Ω around its static resonant frequency ω_0 with an amplitude of δ_ω.

$$\omega_r(t) = \omega_0 + \delta_\omega \cos\{\Omega(t-d)\}, \tag{4}$$

where d is an arbitrary time delay set in the modulation signal. When we deal with CRRs in the later part of this section, multiple values of d are assigned to RRs. With an input light of continuous wave with angular frequency ω and amplitude S_0, i.e., $S_{in}(t) = S_0 \cdot e^{i\omega t}$, (1) becomes

$$\frac{da(t)}{dt} = \left[i\,\{\Delta_\omega + \delta_\omega \cos\Omega(t-d)\} - \frac{1}{\tau} \right] a(t) + \mu S_0, \quad \text{where} \quad \mu = \sqrt{\frac{2}{\tau_c}}. \tag{5}$$

We defined a frequency detuning of $\Delta_\omega = \omega_0 - \omega$ and a slowly-varying amplitude $a(t)$ when $A(t) = a(t)\, e^{i\omega t}$. Hereafter, we used a net photon lifetime of the RR, τ, which is the principal parameter that governs the dynamic response of the RR.

#172056 - $15.00 USD Received 5 Jul 2012; revised 23 Aug 2012; accepted 23 Aug 2012; published 10 Sep 2012

$$\frac{1}{\tau} = \frac{1}{\tau_c} + \frac{1}{\tau_l}. \tag{6}$$

Equation (5) is a linear ordinary differential equation. The solution of Eq. (5) is analytically given in integral form as follows:

$$a(t) = e^{b(t)} \int_0^t e^{-b(x)}\, \mu S_0 dx, \tag{7}$$

$$\begin{aligned} \text{where} \quad b(x) &= \int_0^x \left[i\Delta_\omega + i\delta_\omega \cos\{\Omega(t-d)\} - \frac{1}{\tau} \right] dt \\ &= \left(i\Delta_\omega - \frac{1}{\tau} \right) x + i\frac{\delta_\omega}{\Omega} \left[\sin\{\Omega(x-d)\} + \sin(\Omega d) \right]. \end{aligned} \tag{8}$$

In the above formula, we used the initial condition of $a(0) = 0$. Throughout the analysis, we used a small signal approximation, which means that we only consider the first order of δ_ω. Therefore, to perform the integral in Eq. (7), we apply:

$$e^{-\frac{i\delta_\omega}{\Omega}\left[\sin\{\Omega(t-d)\}+\sin(\Omega d)\right]} \approx 1 - \frac{i\delta_\omega}{\Omega}\left[\sin\{\Omega(t-d)\} + \sin(\Omega d)\right]. \tag{9}$$

By using the approximation of Eq. (9), the integral in Eq. (7) is calculated for a sufficiently large t, as follows:

$$\begin{aligned} \frac{S_{out}\cdot e^{-i\omega t}}{S_0} &= \left(-1 + \frac{\mu^2\tau}{h}\right) + \delta_\omega\tau\frac{\mu^2\tau}{2\Omega\tau}\left(\frac{1}{h} - \frac{1}{h+i\Omega\tau}\right)e^{i\Omega(t-d)} + \delta_\omega\tau\frac{\mu^2\tau}{2\Omega\tau}\left(\frac{1}{h-i\Omega\tau} - \frac{1}{h}\right)e^{-i\Omega(t-d)} \\ &= F^{(0)}\left(\mu^2\tau, \Delta_\omega\tau\right) + \delta_\omega\tau\, F^{+}\left(\mu^2\tau, \Delta_\omega\tau, \Omega\tau\right)e^{i\Omega(t-d)} + \delta_\omega\tau\, F^{-}\left(\mu^2\tau, \Delta_\omega\tau, \Omega\tau\right)e^{-i\Omega(t-d)}, \end{aligned} \tag{10}$$

where we define $h = 1 - i\Delta_\omega\tau$. Equation (10) expressed the frequency response of RR for small signal modulation with an arbitrary choice of the parameter sets of τ, μ, Δ_ω, and Ω. Note that μ, Δ_ω, δ_ω, and Ω are all normalized by τ in the above equation, with the exception of exponential terms. The right hand side of Eq. (10) contains three terms. The first term is the static solution of RR, while the second and third terms are frequency components with angular frequencies of $\omega \pm \Omega$, respectively. These two components are created as side-band components around ω due to the modulation of Ω. Because of the small signal approximation, the side bands of $\omega \pm 2\Omega$, $\omega \pm 3\Omega$, ..., which have higher orders of δ_ω, do not appear in Eq. (10). We introduced three functions, $F^{(0)}(\mu^2\tau, \Delta_\omega\tau)$, $F^{+}(\mu^2\tau, \Delta_\omega\tau, \Omega\tau)$, and $F^{-}(\mu^2\tau, \Delta_\omega\tau, \Omega\tau)$, which correspond to the three terms, as in the second line in Eq. (10).

2.1 SRR-SSM

The response of SRR-SSM has already been reported in other works [22–25]. We present it for comparison purposes with the results for CRR-MZM. In Eq. (10), we reduced the variables by substituting $\mu^2\tau = 1$ and $\Delta_\omega\tau = 1$. The former indicates a condition of the critical coupling, i.e., $\tau_c = \tau_l$ [27]. The latter condition concerns the detuning of the angular frequency between the input light and the resonance of RR. With $\Delta_\omega\tau = 1$, the output in a static solution from the RR is equal to one half of the input power. By substituting these formulas in Eq. (10), for $S_0 = 1$, we obtained

#172056 - $15.00 USD Received 5 Jul 2012; revised 23 Aug 2012; accepted 23 Aug 2012; published 10 Sep 2012

$$|S_{out}|^2 = \frac{1}{2} + \delta_\omega \tau \sqrt{\frac{(\Omega\tau)^2 + 1}{(\Omega\tau)^4 + 4}} \sin\{\Omega(t-d) + \varphi_0\}. \quad (11)$$

$|S_{out}|^2$ varies with the angular frequency of Ω, and its amplitude decreases with Ω, which is inversely proportional to $\Omega\tau$ for large $\Omega\tau$.

2.2 CRR-MZM

Next, we derive the response of CRR-MZM. Figure 2 schematically shows the approach that we used to analyze CRR. At the first left-most RR, continuous light with ω is inputted, and three frequency components are created, as indicated by black bold arrows in Fig. 2 and Eq. (10). We can consider these three components as the input to the second RR, and as continuous waves with frequencies ω and $\omega \pm \Omega$, respectively. Therefore, Eq. (10) can be re-applied to each of these three components to calculate their respective outputs. At the second RR, the inputs with a frequency of $\omega \pm \Omega$ may create frequency components of ω and $\omega \pm 2\Omega$, respectively. However, these four components are all for second-order terms about δ_ω,, and are therefore neglected in small-signal analysis. Consequently, the second RR also outputs continuous lights with frequencies of ω and $\omega \pm \Omega$. By making this speculation regarding the following RRs, it is noted that even for CRR with $N > 2$, the frequency components with ω and $\omega \pm \Omega$ are enough to be considered for our small signal analysis; the input and output of the j-th RR both have three frequency components of ω and $\omega \pm \Omega$. As shown in Fig. 2, we defined the amplitude of the outputs from the j-th RR with frequencies ω, $\omega + \Omega$, and $\omega - \Omega$ as $a_j^{(0)}$, a_j^+, and a_j^-, respectively. Next, we derive a recurrence formula for $a_j^{(0)}$, a_j^+, and a_j^-. The red bold arrows correspond to the dependencies of $a_j^{(0)}$, a_j^+ and a_j^- on those in the previous step. Obviously, a_{j-1}^+ and a_{j-1}^- are at least with the first order of δ_ω, and therefore, they only affect a_{j-1}^+ and a_{j-1}^-, and $a_j^{(0)}$ is therefore determined only by $a_{j-1}^{(0)}$. The red arrows in Fig. 2 indicate the remaining dependencies which we have to consider. The coefficients are determined by Eq. (10). As a result, we obtained

$$a_j^\pm = F^{(0)}\left(\mu^2\tau, \mp\Omega\tau\right) a_{j-1}^\pm + \delta_\omega \tau\, F^\pm\left(\mu^2\tau, 0, \Omega\tau\right) e^{\mp i\Omega(j-1)d}\, a_{j-1}^{(0)}, \quad \text{and} \quad (12a)$$

$$a_j^{(0)} = F^{(0)}\left(\mu^2\tau, 0\right) a_{j-1}^{(0)}, \quad (12b)$$

with initial values of $a_0^{(0)} = 1$ and $a_0^\pm = 0$. As shown in Fig. 1(c), we assumed a constant time delay of d between all pairs of neighboring RRs, which adds a phase factor of $e^{\pm i\Omega(j-1)d}$ to $\alpha_j^\pm$ as in Eq. (12a). In addition, CRR-MZM uses each RR as a phase modulator. The phase change is most enhanced at the resonant frequencies of the RRs, and we therefore set the detuning as $\Delta_\omega = 0$ [8, 10]. Note that the above recurrence formulas automatically confine the analysis to within the first order of δ_ω and the frequency components of ω and $\omega \pm \Omega$.

The expression of a_N is obtained from Eq. (12a) and (12b) as follows:

$$a_N^\pm = \delta_\omega \tau\, F^\pm\left(\mu^2\tau, 0, \Omega\tau\right) \sum_{j=1}^{N} \left[e^{\mp i\Omega(N-j)d} \left\{F^{(0)}\left(\mu^2\tau, 0\right)\right\}^{N-j} \left\{F^{(0)}\left(\mu^2\tau, \mp\Omega\tau\right)\right\}^{j-1} \right]. \quad (13a)$$

$$a_N^{(0)} = \left\{F^{(0)}\left(\mu^2\tau, 0\right)\right\}^N. \quad (13b)$$

As shown in Fig. 1(c), CRRs are loaded as phase modulators on each arm of the Mach-Zehner interferometer. The two CRRs are operated by the signals having opposite polarities. When the static phase difference of $\pi/2$ is given between two arms, the output S_{out} from the CRR-MZM in Fig. 1(c) becomes

#172056 - $15.00 USD Received 5 Jul 2012; revised 23 Aug 2012; accepted 23 Aug 2012; published 10 Sep 2012

$$S_{out}\, e^{-i\omega t} = \frac{1}{2}\left[\alpha_N^{+}\, e^{i\Omega t} + \alpha_N^{(0)} + \alpha_N^{-}\, e^{-i\Omega t}\right] + \frac{i}{2}\left[-\alpha_N^{+}\, e^{i\Omega t} + \alpha_N^{(0)} - \alpha_N^{-}\, e^{-i\Omega t}\right]. \quad (14)$$

Unlike SRR-SSM, CRR-MZMs do not need the condition of critical coupling, and the propagation loss of the waveguide is ideally zero for the maximum output from the modulator. When we consider the loss-less case, $1/\tau_l = 0$, $\mu^2\tau = 2$, and $F^{(0)}(\mu^2\tau,0) = 1$. With all of these simplifications, we obtained

$$\left|S_{out}\right|^2 = \frac{1}{2} + \delta_\omega\tau\,\frac{2}{\sqrt{1+(\Omega\tau)^2}}\left|\sum_{j=1}^{N} e^{i(\Omega d - 2\theta)j}\right| \sin\left\{\Omega t + \varphi'(\Omega)\right\}, \quad \text{where} \quad \tan\theta = \Omega\tau, \quad (15)$$

as the response of CRR-MZM. For the single RR case, i.e., $N = 1$, the summation becomes unity in the above equation. In this case, the amplitude of $\sin(\Omega t + \varphi')$ decreases with Ω, and is inversely proportional to $\Omega\tau$ for large $\Omega\tau$, which is similar to the case with SRR-SSM. In the case of CRRs, i.e., $N > 1$, the summation part is not equal to unity, and represents the distortion of the frequency response of CRR-MZM due to the cascading of RRs.

Using Eq. (15), we consider the optimized configuration of CRR-MZM to maximize its response at a given operating frequency. First, it is reasonable to design each RR so that $\Omega\tau << 1$, to obtain a sufficiently large modulator bandwidth for a given Ω. In this case, the response of each RR may be small, as was observed in Eq. (15) for $N = 1$. Therefore, we should cascade RRs to accumulate the phase change and to obtain a sufficient modulator response. The important thing here is to choose a proper delay d to minimize the effect of the summation in Eq. (15). Because we chose τ so that $\Omega\tau << 1$, then $\theta \approx \Omega\tau$ in Eq. (15). Consequently, if the delay $d = 2\tau$, the summation in Eq. (15) becomes N regardless of the frequency Ω. In this case, the impact of cascading RR on the response becomes a simple multiplication with a factor of N. This choice of delay is considered to be an optimized value required for CRR-MZMs to minimize the distortion in the frequency response. This result is reasonable because the group delay of each RR is also equal to 2τ.

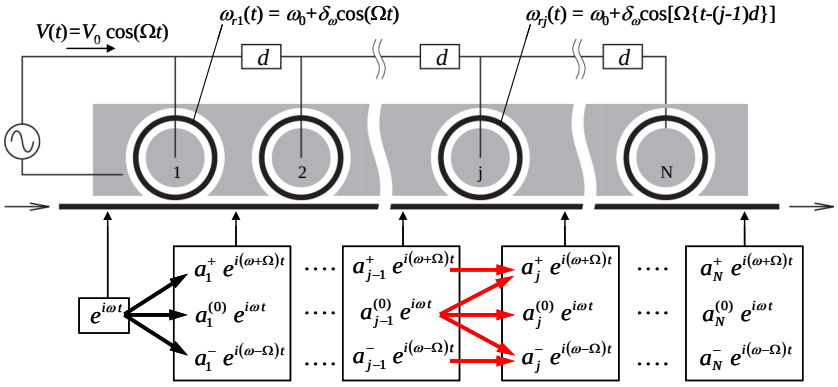

Fig. 2. Schematic structure of phase modulator based on CRRs (top) and calculation diagram for small signal responses (bottom). In each RR, three frequency components of light are created in small signal analysis. One is the input light with angular frequency ω, and the others are with $\omega \pm \Omega$, which are side-bands that were created around ω due to the modulation. $a_j^{(0)}$ and $a_j^{\pm}$ are the amplitude of those frequency components. The bold arrows indicate the dependencies of these three frequency components on those at the previous RR at the first (black) and j-th RR (red), respectively.

Figure 3 shows the calculated frequency responses of SRR-SSM and CRR-MZM, which were obtained using Eqs. (11) and (15). The response was defined as the amplitude of the sinusoidal term in $|S_{out}|^2$ divided by $\delta_\omega\tau$. SRR-SSM and SRR-MZM (CRR-MZM for $N = 1$) have a similar dependence on $\Omega\tau$. For large $\Omega\tau$, both decrease at a rate of −10 dB/decade, as

#172056 - $15.00 USD Received 5 Jul 2012; revised 23 Aug 2012; accepted 23 Aug 2012; published 10 Sep 2012

shown by the black and green curves in Fig. 3. With respect to 10-CRR-MZMs, their responses are 10 times larger than that of SRR-MZM for the smallest $\Omega\tau$, regardless of the delay d, as shown by the blue and red curves in Fig. 3. However, the bandwidth of 10-CRR-MZM is much smaller than that of SRR-MZM with $d = 0$, as shown by the blue curve. As expected, the bandwidth is much improved for 10-CRR-MZM with $d = 2\tau$, and is comparable to that of SRR-MZM. If we compare 10-CRR-MZM with $d = 2\tau$ to standard SRR-SSM, the former shows a much larger response at small $\Omega\tau$ with a smaller modulation bandwidth, as shown in Fig. 3. In the next section, we compared both configurations with respect to response at low frequencies and the modulation bandwidth, using a wide range of parameter sets, including the propagation loss of the waveguide and τ and N.

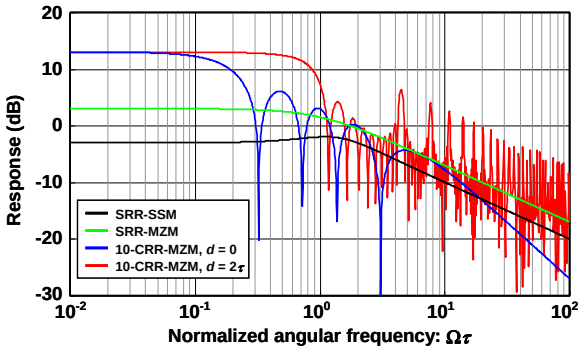

Fig. 3. Calculated small-signal response of SRR-SSM (black) and CRR-MZMs with single (green) or 10 RRs (blue and red) on each arm. The modulation frequency is normalized by the photon lifetime of RR. For one of the 10 CRR-MZMs (blue), modulation signals are applied to the RRs with the same timing, whereas a delay of $d = 2\tau$ is set in signals between neighboring RRs for the other (red).

3. Numerical calculations

In this section, we show the calculated results of the response of CRR-MZM with a wide variety of parameter sets. The results are compared with those of standard SRR-SSMs.

3.1 Numerical method

First, we performed numerical calculations to confirm the validity of the analysis in the previous section. The configuration is summarized for SRR in Fig. 4. We used a slowly-varying-envelope approximation, in which we defined the lightwave propagating along the ring waveguides as $U(t, z) = u(t, z)\, e^{i(\omega t - kz)}$. $u(t, z)$ is a slowly varying function when compared with the angular frequency of light ω, and satisfies the following partial differential equation [28]:

$$\frac{1}{v_g}\frac{\partial u}{\partial t} + \frac{\partial u}{\partial z} = 0. \tag{16}$$

In the coupling region, we considered the boundary condition as follows:

$$u_1(t) = y\, u_2(t)\, e^{-\alpha(2\pi R)+i\varphi(t)} - i\sqrt{1-y^2}\, u_0(t). \tag{17a}$$

$$u_3(t) = y\, u_0(t) - i\sqrt{1-y^2}\, u_2(t)\, e^{-\alpha(2\pi R)+i\varphi(t)}. \tag{17b}$$

The term $-\alpha(2\pi R) + \varphi(t)$ means the attenuation and phase shift that are experienced by the light in the RR.

#172056 - $15.00 USD Received 5 Jul 2012; revised 23 Aug 2012; accepted 23 Aug 2012; published 10 Sep 2012

To solve Eq. (16) and (17) numerically, we discretized time by the round-trip time $\tau_0 = (2\pi R\, n_g)/c$ as $t = t_m = m\tau_0$. Note that in these calculations, we neglected variations of $u(t)$ in the RR that were faster than τ_0. As in the analysis in the previous section, we also neglected the modulation of the group index in the waveguide. With these assumptions from Eq. (16),

$$u_2(t_m) = u_1(t_{m-1}). \tag{18}$$

We numerically solved the above equations for the first RR with a constant input $u_1(t) = 1$. The outputs obtained from the first RRs were used as the inputs of the successive RR. The modulation of the j-th RR was defined in the $\varphi(t)$ as

$$\varphi(t) = \frac{\Delta_\omega + \delta_\omega \cos\left\lfloor \Omega\{t-(j-1)d\}\right\rfloor}{f_{FSR}}, \tag{19}$$

where f_{FSR} refers to the free-spectral range of the RR in frequency and Δ_ω and δ_ω are the same as in the previous section. For these modulation signals, we calculated the optical output power from CRR-MZMs. For sufficiently large t, the optical output power varied sinusoidally with Ω regardless of the modulator configuration or the initial state, and we extracted its amplitude as the response $\Delta P(\Omega)$ of the modulator.

Figure 5 shows the response of CRR-MZMs calculated using both analytical and numerical methods. The results coincided with each other when the resonance was sharp with a relatively small 1-y^2 (5%), which confirms the validity of the analysis in the previous section. The responses were slightly different when the resonance was broad with a relatively large 1-y^2 (40%). This deviation at a large 1-y^2 occurred because the TCM theory is only valid for the resonators which weakly couple to the outside [26]. Although the analysis in the previous section is useful to gain an insight into the dynamics in CRR-MZMs, it should be carefully applied to obtain quantitative results, especially for relatively low-Q RRs. In the rest of paper, we show the results calculated using the numerical model to include low-Q RRs. In fact, 2τ, which was calculated using Eqs. (3) and (6), is equal to the group delay of RR at $\Delta_\omega = 0$, for only high-Q RRs. A more rigorous expression of the group delay of RR was given in previous works [29]. For the numerical calculations in this paper, we used the delay d that was calculated by this rigorous form, and inserted it in signals between two adjacent RRs.

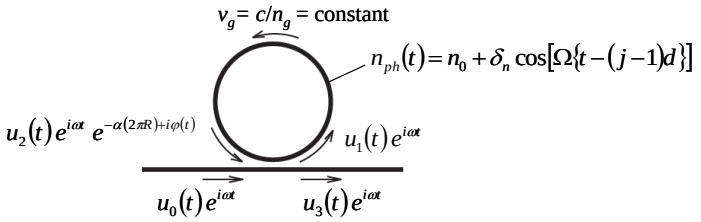

Fig. 4. Configuration and definition of variables used in numerical calculations to obtain the response of a single RR.

#172056 - $15.00 USD Received 5 Jul 2012; revised 23 Aug 2012; accepted 23 Aug 2012; published 10 Sep 2012

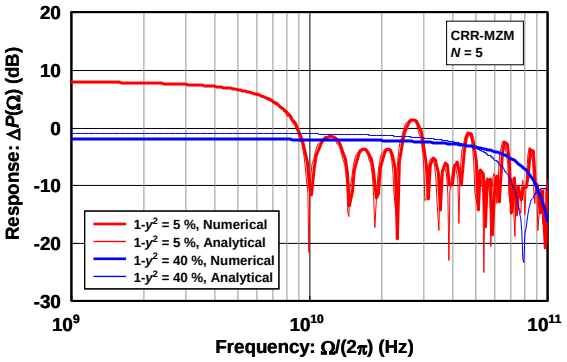

Fig. 5. Comparison of calculated responses of CRR-MZM with N = 5, between analytical (narrow) and numerical (bold) methods, for relatively small-coupling high-Q RR with $1\text{-}y^2$ = 5% (red) and large-coupling low-Q RR with $1\text{-}y^2$ = 40% (blue).

3.2 Calculated performance comparison between SRR-SSM and CRR-MZM

We numerically calculated the DC response $\Delta P_{DC} = \Delta P(0)$ and the 3-dB bandwidth of SRR-SSMs and CRR-MZMs. Table 1 summarizes the conditions of the calculations. As shown in Table 1, we directly assigned values to some of the parameters, whereas the others were calculated from those values indicated in the table. We used the same conditions of the frequency detuning for SRR-SSM and CRR-MZM as mentioned in sections 2.1 and 2.2, respectively. We determined the values of n_g, R, and α_{dB} by making reference to other studies on silicon-based modulators [2–10].

Table 1. Conditions of numerical calculations

Parameter	Notation	SRR-SSM	CRR-MZM
Group index of waveguide	n_g	4	
Perimeter of RR	$2\pi R$	50 μm	
Round-trip time	$\tau_0 = (2\pi R\, n_g)/c$	0.67 ps	
Photon lifetime of RR	τ	2 – 200 ps	
Frequency detuning between input light and resonance of RR.	Δ_ω	$1/\tau$	0
Propagation loss in waveguide	α_{dB}	-[a]	0 or 10 dB/cm
Coupling coefficient	$1\text{-}y^2$	-[b]	-[c]
Number of RRs	N	1	1, 4, or 16[d]
Amplitude of resonant-frequency variation	$\delta_\omega/(2\pi)$	3.9 GHz	

[a]Calculated from the critical-coupling condition as $\tau_c = 2\tau$ and Eq. (3a).
[b]Calculated from the critical-coupling condition as $\tau_c = \tau_l$ and Eq. (3b).
[c]Calculated from Eqs. (3a), (3b), and (6) with values of τ and α_{dB}.
[d]N refers to the number of RRs cascaded and loaded onto each of the two bus waveguides in the interferometer; CRR-MZM contains $2N$-RRs in total.

Figure 6 shows the calculated results for SRR-SSM, and CRR-MZMs with α_{dB} = 0 and different values of τ and N. The left axis is the response of the modulators to a DC input, which was analytically calculated by Eqs. (17) and (18) using static solutions. The right axis indicates the 3-dB bandwidth, f_{3dB}, at which the response $\Delta P(\Omega)$ becomes half of the DC response ΔP_{DC}. Figure 6(a) shows general dependencies in RR-based modulators, regardless of the structures of the modulators in which the DC responses increase with the photon lifetime of the RR, whereas the 3-dB bandwidths decrease. The slopes of the DC response are constant for an increasing photon lifetime, and are almost the same among different structures. For a constant lifetime, the differences between the red, green, and blue solid curves are about 6-dB, corresponding to N = 1, 4, and 16 for CRR-MZMs. This means that an increase of the response by N-times is obtained for CRR-MZMs with N-CRRs. However, in this case, the 3-dB bandwidths decrease with increasing N, as shown by the dashed curves. To

#172056 - $15.00 USD Received 5 Jul 2012; revised 23 Aug 2012; accepted 23 Aug 2012; published 10 Sep 2012

compare the results on the same basis, we drew parametric plots between the DC response and the 3-dB bandwidth with the parameter of the photon lifetime, as shown in Fig. 6(b). As clearly shown in the graph, CRR-MZMs have a greater response with an increase in N for a constant 3-dB bandwidth, which confirms our predictions for CRR-MZMs which were mentioned in the introduction of this paper. Without propagation loss of the RRs, these gains are preserved at any 3-dB bandwidth. In other words, they are independent of the photon lifetime of the RRs.

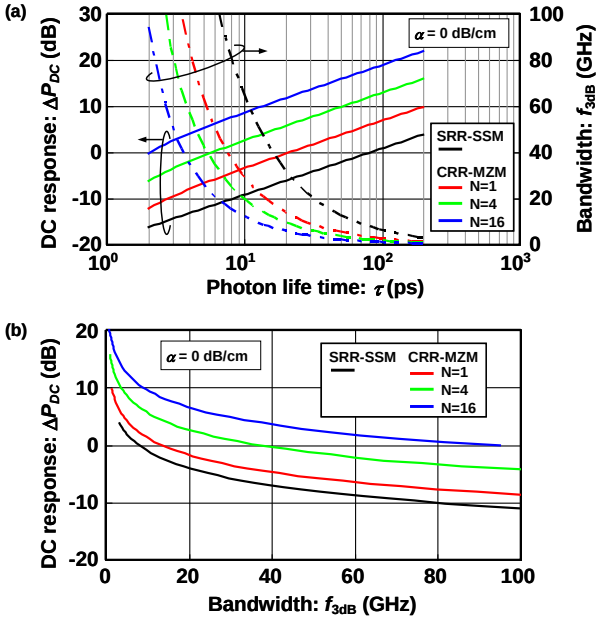

Fig. 6. (a) Calculated DC response (solid) and 3-dB bandwidth (dashed) of SRR-SSM (black) and CRR-MZM (red, green, and blue) for an RR photon lifetime of 0.2-200 ps. No propagation loss is assigned to the waveguide for CRR-MZMs, whereas loss that causes critical coupling is assigned to SRR-SSM. (b) Parametric plot between DC response and 3-dB bandwidth using photon lifetime as the parameter.

In reality, RRs are always accompanied by a certain amount of propagation loss due to side-wall scattering and radiation in the curved waveguides. To investigate the impact of the loss on the design of CRR-MZMs, we calculated the performances of CRR-MZMs with a propagation loss of 10 dB/cm assigned to the RRs. In this case, we neglected loss of the bus waveguide because such loss is usually much smaller than those in RRs. In RRs, light propagates effectively long waveguides due to the resonance and those waveguides are supposed to be lossy due to dopants and electrode. By contrast, the bus waveguide is passive and non-resonant. Therefore, the bus waveguide will give only minor impact on the modulation characteristics of the CRR-MZM in terms of loss when necessary and sufficient spaces are given between neighboring RRs. As such space, about 20 μm would be sufficient for RRs with several-micron radius [10].

As a result, the DC responses showed much different behaviors from those without losses, whereas the dependences of the 3-dB bandwidth on the photon lifetime were almost the same as those without losses. Unlike the loss-less case, the DC responses showed decreases with relatively large photon lifetime values for CRR-MZMs, as shown by the red, green, and blue solid curves in Fig. 7(a). This dependence is caused by the enhancement of the loss in RRs. When the lifetime increases towards the critical coupling, both the loss and phase shift are enhanced. The transmitted power from RRs exponentially decreases with this enhancement factor and the number of RRs, whereas the phase-change only linearly increases with those parameters. The balance between them determines the overall dependencies of the DC

#172056 - $15.00 USD Received 5 Jul 2012; revised 23 Aug 2012; accepted 23 Aug 2012; published 10 Sep 2012

response of RRs and the maximum achievable response at a specific photon lifetime. Note that the photon lifetime which gives the maximum DC response decreases with *N*, as shown in Fig. 7(a). Figure 7(b) is the parametric plot of the photon lifetime, and corresponds to Fig. 6(b). For a 3-dB bandwidth smaller than 25 GHz, CRR-MZMs have a relatively smaller DC response when compared with the SRR-SSM, regardless of *N*, and the strategy of cascading RRs does not work. This is due to the large photon lifetime and the enhancement of loss in RRs. However, this dependence is not the case for a large 3-dB bandwidth with a relatively small photon lifetime. For a 3-dB bandwidth larger than 25 GHz, the modulation of CRR-MZM accumulates with an increase of *N*, and CRR-MZMs provide larger responses than those provided by SRR-SSM, as shown in Fig. 7(b). Therefore, cascading RRs are still more effective than SRR-SSM for obtaining larger responses at high frequencies, even with the propagation losses.

Throughout this paper, we assumed that a constant amplitude of the resonant-frequency shifts was induced in each RR by refractive index modulation. This situation implied that the electrical signals applied to the RRs had constant voltage amplitudes. Such a voltage amplitude is limited in most applications. In particular, when the driver circuits are based on CMOS technologies, a voltage amplitude in the sub-volt range is required. With this constraint, CRR-MZMs have a degree of freedom in their design that increases the modulation response for high-operating frequencies by cascading RRs with a relatively small photon lifetime. This approach may be considered to be a compromise because the power consumption would increase with the number of RRs driven. Even so, this approach is useful, given that the standard SRR-SSM would fail to provide sufficient modulation of light at high-frequencies due to its limited configuration. In addition, note that as long as *y* is less than 1, the presence of the RRs ensures that there is some enhancement of the phase modulation in the CRR-MZM with a factor of τ/τ_0, when compared with the standard non-resonant Mach-Zehnder modulator [10].

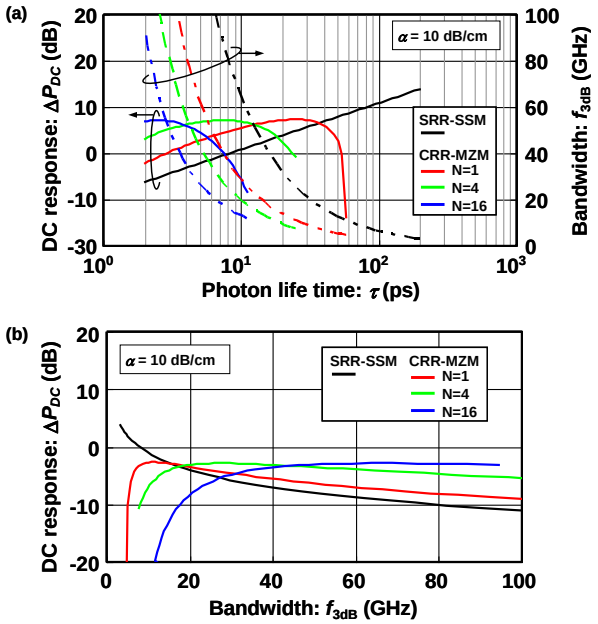

Fig. 7. (a) Calculated DC response (solid) and 3-dB bandwidth (dashed) of SRR-SSM (black) and CRR-MZM (red, green, and blue), for photon lifetime of RR of 0.2-200 ps. A propagation loss of α_{dB} = 10 dB/cm is assigned to the waveguide for CRR-MZMs, whereas loss cause critical coupling is assigned to SRR-SSM. (b) Parametric plot between DC response and 3-dB bandwidth using photon lifetime as parameter.

#172056 - $15.00 USD Received 5 Jul 2012; revised 23 Aug 2012; accepted 23 Aug 2012; published 10 Sep 2012

Finally, we calculated the output waveforms from SRR-SSM and CRR-MZM for a 50-Gb/s pseudorandom binary sequence (PRBS) of 2^7-1. In the calculation, we used the same procedure as that described in section 3.1. The use of Eqs. (16) to (18) is not limited within small signal analysis and is valid for large signal modulation. Therefore, we simply applied the input signals of PRBS to those equations and the procedure to calculate eye diagrams. We set the rise and fall time to be 5.9 ps for the transition between 0 and 1 state with the thresholds of 10 and 90%, respectively. This rise/fall time was large enough for the round-trip time of 0.67 ps. By using Fig. 7(a), we determined the photon lifetimes of the RRs used in the two device configurations, respectively, such that both devices had the same 3-dB bandwidth of about 40 GHz. With this constant 3-dB bandwidth, it is expected that both devices equally show sufficient qualities of eye diagrams for 50-Gb/s operations. Thus, it is possible to evaluate the modulation depths of the two devices and compare them for 50-Gb/s operations. Choice of the smaller 3-dB bandwidth and the longer photon lifetimes would cause inadequate qualities of eye diagrams for 50-Gb/s operations. Figures 8(a) and (b) show the resulting eye diagrams, with the parameters used in the calculation shown in the graphs. By cascading 4-RRs with a relatively small photon lifetime, the CRR-MZM provided an eye opening that was wider than that of the SRR-SSM.

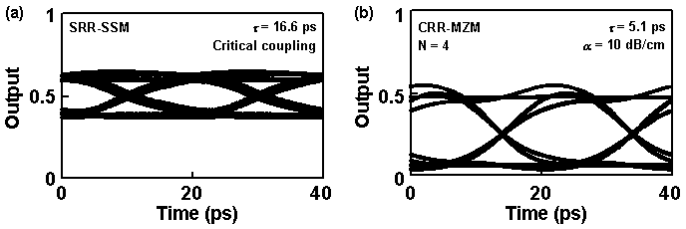

Fig. 8. Calculated outputs as eye diagrams for 50-Gb/s PRBS signal of 2^7-1. (a) SRR-SSM (b) CRR-MZM with $N = 4$ (b).

4. Conclusion

We investigated the high-speed modulation characteristics of CRR-MZMs using analytical and numerical calculations. We derived an analytical formula for the small-signal response of CRR-MZM based on TCM theory, for which we numerically confirmed the validity. The analysis indicated that CRR-MZMs had a maximum operating bandwidth when proper delays were set in the applied electrical signals between neighboring RRs. The optimized delay was equal to twice the photon lifetime of each RR.

We determined the performances of both CRR-MZMs and standard SRR-SSM for a wide variety of parameters, including the photon lifetime of RRs, the number of RRs cascaded, and the propagation loss of the RR. We compared the results between those two device configurations in terms of the modulation depth and bandwidth. For a given magnitude of the waveguide index change, CRR-MZM can provide a larger modulation response than an SRR-type modulator in a frequency range greater than 25 GHz. The results showed the advantage of CRR-MZM over SRR-SSM in designs aimed at providing a larger modulation response at high-operating frequencies.

Acknowledgments

The authors would like to thank Tatsuya Usuki for the helpful discussions and suggestions that he made. The authors also acknowledge valuable assistance from Tsuyoshi Yamamoto.

#172056 - $15.00 USD Received 5 Jul 2012; revised 23 Aug 2012; accepted 23 Aug 2012; published 10 Sep 2012